



LAWRENCE
LIVERMORE
NATIONAL
LABORATORY

X-Ray Scattering Measurements of Strong Ion-Ion Correlations in Shock-Compressed Aluminum

T. Ma, T. Doeppner, T. W. Falcone, L. Fletcher, C.
Fortmann, D. O. Gericke, O. L. Landen, H. J. Lee, A.
Pak, J. Vorberger, K. Wunsch, S. H. Glenzer

November 28, 2012

Physical Review Letters

Disclaimer

This document was prepared as an account of work sponsored by an agency of the United States government. Neither the United States government nor Lawrence Livermore National Security, LLC, nor any of their employees makes any warranty, expressed or implied, or assumes any legal liability or responsibility for the accuracy, completeness, or usefulness of any information, apparatus, product, or process disclosed, or represents that its use would not infringe privately owned rights. Reference herein to any specific commercial product, process, or service by trade name, trademark, manufacturer, or otherwise does not necessarily constitute or imply its endorsement, recommendation, or favoring by the United States government or Lawrence Livermore National Security, LLC. The views and opinions of authors expressed herein do not necessarily state or reflect those of the United States government or Lawrence Livermore National Security, LLC, and shall not be used for advertising or product endorsement purposes.

X-Ray Scattering Measurements of Strong Ion-Ion Correlations in Shock-Compressed Aluminum

T. Ma,¹ T. Döppner,¹ R. W. Falcone,² L. Fletcher,² C. Fortmann,^{1,3} D. O. Gericke,⁴
O. L. Landen,¹ H. J. Lee,⁵ A. Pak,¹ J. Vorberger,⁴ K. Wünsch,⁴ and S. H. Glenzer¹

¹*Lawrence Livermore National Laboratory, Livermore, CA 94550, USA*

²*Physics Department, University of California, Berkeley, CA 94720, USA*

³*Department of Physics and Astronomy, University of California, Los Angeles, CA 90095, USA*

⁴*Centre for Fusion, Space and Astrophysics, Department of Physics,
University of Warwick, Coventry CV4 7AL, United Kingdom*

⁵*Stanford Linear Accelerator Center, Menlo Park, CA 94309, USA*

(Dated: September 18, 2012)

The strong ion-ion correlation peak characteristic of warm dense matter (WDM) is observed for the first time using simultaneous angularly, temporally, and spectrally resolved x-ray scattering measurements in laser-driven shock-compressed aluminum. Laser-produced molybdenum x-ray line emission at an energy of 17.9 keV is employed to probe aluminum compressed to a density of $\rho > 8 \text{ g/cm}^3$. We observe a well pronounced peak in the static structure factor at a wave number of $k = 4.0 \text{ \AA}^{-1}$. The magnitude of this correlation peak is in contradiction to the usual plasma theories employing a linear screened potential but is in good agreement with calculations using a potential with strong short range repulsion.

PACS numbers: 52.50.Jm, 52.25.Os, 52.27.Gr, 52.65.Yy

The accurate characterization of material properties under extreme conditions is important for the understanding of high energy density states of matter, ranging from planetary interiors to capsule implosions for inertial confinement fusion (ICF). Typically, x-ray Thomson scattering (XRTS) experiments have been conducted on low-Z, moderately compressed materials. However, recent progress on the National Ignition Facility (NIF) has yielded $> 600\times$ compression of ICF ablator materials [1, 2], and > 100 Mbar compression of tantalum, spurring intense interest in high energy XRTS > 10 keV to make it possible to penetrate and characterize these very dense states of matter.

Aluminum, a well-studied mid-Z element [3–8], serves as an excellent material for which to validate theoretical models that predict strong correlations very different from the ideal or weakly coupled plasma behavior, and which are expected in the warm dense matter regime [9, 10]. XRTS has been shown to robustly provide direct and accurate measurements of thermodynamic and physical properties, and can be applied as a non-invasive first principles technique to determine the state of compression [11–13]. This type of extensive momentum-resolution of spectrally and angularly resolved XRTS has not previously been used in WDM research and is critically needed to test detailed dense plasma modeling. Using this method to garner information on the dynamic structure factor, $S(k, \omega)$, we can infer basic material properties such as conductivity, stopping power, and energy transfer rates, as the determining physical quantity is in all cases the density response function [14].

In this Letter, we present high-energy x-ray scattering experiments in which tailored shocks are driven into solid

aluminum targets to induce high compression (three-fold solid density). Then, molybdenum $2p \rightarrow 1s$ x-ray line emission centered at 17.9 keV is used as a probe to perform scattering in the non-collective regime over a range of scattering angles. This high-energy angularly resolved XRTS technique probes the ion-ion correlation peak whose angular position directly provides the distance between the two nearest neighbors and consequently the mass density of the compressed Al.

From momentum and energy conservation, the angle at which x-rays scatter from electrons, probing the dynamic structure factor at various wave vectors \mathbf{k} , is given by,

$$k = |\mathbf{k}| = \frac{4\pi E_0}{hc} \sin \frac{\theta_s}{2} \quad (1)$$

where $E_0 = 17.9$ keV is the incident energy of the x-rays applied here, θ_s is the scattering angle, h is Planck's constant and c the speed of light. Such Thomson scattering is characterized by the scattering parameter α ,

$$\alpha = \frac{1}{k\lambda_s} \quad (2)$$

where λ_s is the screening length. In the non-degenerate case, λ_s is the standard Debye screening length, but in degenerate systems (as in this experiment) it is the Thomas-Fermi screening length. Here, both forward and backward scattering is used to achieve scattering angles from 25° to 130° (comprising wave numbers of $4.0 \text{ \AA}^{-1} < k < 16.4 \text{ \AA}^{-1}$), corresponding to a scattering parameter α in the interval $0.12 < \alpha < 0.52$, indicating non-collective scattering.

The full spectral x-ray scattering response [15, 16] can be described by the total electron dynamic structure factor, which allows the following decomposition

$$S(k, \omega) = |f(k) + q(k)|^2 S_{ii}(k) \delta(\omega) + Z_f S_{ee}(k, \omega) + Z_C \int S_{CE}(k, \omega - \omega') S_S(k, \omega') d\omega'. \quad (3)$$

Here, $f(k)$ is the ion form factor, $q(k)$ describes the screening cloud, $S_{ii}(k)$ is the static ion structure factor and $S_{ee}(k, \omega)$ is the dynamic structure factor of the free electrons in the system. The response of the bound electrons in the system is described in part by the first term of Eq. (3) where the ion form factor is convolved with the ion structure factor. The free electrons in the system are responsible for two features in the total dynamic structure factor: first, the forming of a dynamic screening cloud around the ions is described by the product of $q(k)$ and the static ion structure; second, the spectral feature of free electrons totally independent of any ionic structure, described by the free electron dynamic structure factor. The latter contribution is determined by individual free electrons or collective electronic excitation (plasmons) depending on α . The third term includes inelastic scattering by bound electrons, i.e., bound-free transitions [17].

In the non-collective regime sampled in this experiment, the x-rays are scattered by individual electrons and the total scattered spectrum consists of the elastically scattered component (Rayleigh peak) and inelastically scattered component (Compton peak), where the free electrons determine the width and absolute intensity of the spectral shape. At large scattering vectors, the contribution from electrons in the screening cloud is negligible ($q(k)$ converges to 0) and the strength of the elastic scattering feature approaches $f(k)^2 S_{ii}$. The shift of the Compton peak is determined by the Compton energy $E_C = (hk/2\pi)^2/2m_e$, which in this experiment spans from 60 eV to 1.2 keV.

We perform the experiment on the OMEGA-60 laser at the Laboratory for Laser Energetics [18]. Fig. 1(a) shows a schematic of the experiment. The 125 μm thick aluminum foil targets are compressed from one side with a single strong shock generated using nine laser beams with a total energy of 4.5 kJ in a 1 ns square pulse. Distributed phase plates are used to achieve a smooth ~ 1 mm focal spot, yielding a total drive intensity of 9×10^{14} W/cm² on the sample. 2-D radiation-hydrodynamic calculations using the HYDRA code [19] indicate this laser configuration launches a strong shock wave into the solid target, compressing the aluminum to more than threefold solid density with pressures of 30 – 40 Mbar. Bright, penetrating 17.9 keV Mo 2p \rightarrow 1s transition x-rays are used to probe the compressed Al at approximately 3.0 ns (matched to the shock propagation time to achieve uniform compression throughout the sample). These Mo x-rays are produced using 15 beams of 1 ns duration with an 80 μm focal spot, 500 J per beam, incident on a thin 12 μm molybdenum foil. To enhance the conversion ef-

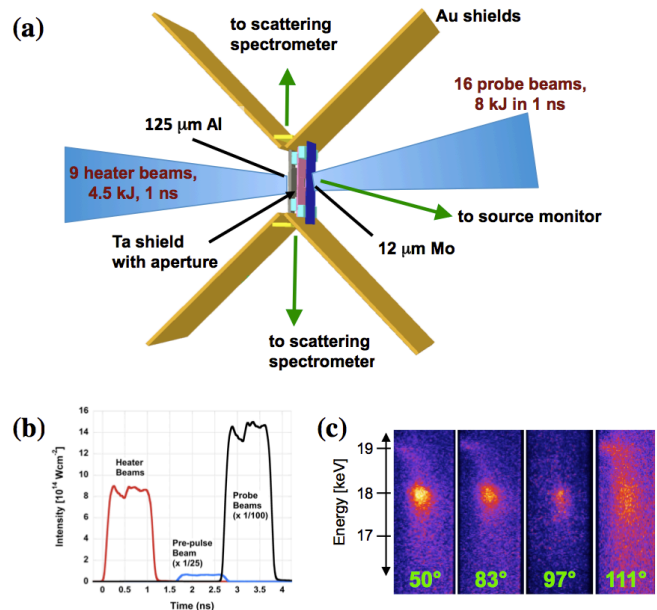


FIG. 1. (a) Schematic of the experiment showing nine heater beams that compress the Al foil and 16 delayed probe beams that produce $E = 17.9$ keV x-rays. X-ray scattering are observed in both the upward and downward directions with gated curved crystal spectrometers. The vertical location of the aperture in the Ta shield defines the two scattering angles on a given shot. (b) Heater, probe, and probe pre-pulse beam intensities on target. (c) Example of the raw scattering data show that the relative intensity of scattering is greatly reduced with increasing angle.

iciency into Mo thermal line radiation [20, 21], a single laser beam defocused to a 200 μm focal spot, 1 ns duration precedes the group of 15 beams by 1 ns to produce a low-density pre-plasma. The laser-to-Mo K-shell x-ray energy conversion efficiency is measured to be $1 - 2 \times 10^{-5}$.

A tantalum aperture of either $200 \times 540 \mu\text{m}$ or $400 \times 540 \mu\text{m}$ between the molybdenum and aluminum foils serves to determine the range of k -vectors probed by selecting the solid angle subtended by the molybdenum x-rays. Further, for any given shot, by moving the vertical location of the aperture relative to the source of molybdenum probe x-rays, the incident probe radiation intersecting the shocked region changes, thus allowing for different scattering angles.

Large gold foils prevent the direct observation of the Mo plasma emission by two curved highly oriented pyrolytic graphite (HOPG) spectrometers [22]. Each of the two HOPG crystals used in the spectrometers that observe the scattering have a radius of curvature of 27 mm and are run in second order, giving a spectral resolution

of $\lambda/\Delta\lambda \sim 175$ for the spectrum centered around the Mo He- α . The crystals are coupled to a microchannel-plate-based gated framing camera with 250 ps temporal resolution.

An absolutely calibrated Transmission Crystal Spectrometer [23, 24] monitors the output of the probe source in first order on each shot. The shot-to-shot variation in x-ray intensity of the Mo K-shell source centered at 17.9 keV is found not to vary by more than 13%, which is taken into account for comparing signal levels from different shots.

An example of the raw scattering data recorded at several scattering angles is shown in Fig. 1(c). The observed total signal is dominated by the elastically scattered photons and shows a strong dependence on the angle of scatter.

Figure 2 shows two examples of the spectrally resolved scattering spectra for 69° ($k = 10.3 \text{ \AA}^{-1}$) and 111° ($k = 15.0 \text{ \AA}^{-1}$). The experimental spectra are background corrected and smoothed over 100 eV. Also shown are the best fits from synthetic spectra generated by convolving Eq. (3) with the experimental instrument function. The individual contributions from elastic, free-free, and bound-free scattering are illustrated. The free electron feature is derived within the random phase approximation [25] and the elastic amplitude is fitted for comparison with detailed theories [26]. For small scattering angles ($25^\circ < \theta_s < 50^\circ$), the total frequency resolved scattering spectrum reflects the source spectrum. For the full set of experimental scattering spectra taken at the various scattering angles, good theoretical fits were found at a mass density of $\rho = 8.1 \text{ g/cm}^3$, electron and ion temperature of $T_e = T_i = 10 \text{ eV}$, and an average ionization state of $Z = 3$. These values are in agreement with the HYDRA radiation-hydrodynamic modeling.

The width of the downscattered inelastic feature is responsive to the relative contributions of the bound-free and free-free feature, which is utilized to infer the number of bound electrons and hence the ionization degree of the plasma. Because the plasma is Fermi-degenerate ($T_e < T_F$), the scattering parameter, α , depends only weakly on the electron density ($\sim n_e^{1/6}$), and is independent of T_e . Thus, the relative intensity ratio between the elastic and inelastic scattering features is almost uniquely a function of the number of free electrons (modifying the screening). The sensitivity of the fits to varying the average ionization, $\langle Z \rangle$, while the mass density is held constant, is shown in the inset of Fig. 2(a). The spectra show that the red shoulder of the inelastic feature is mainly determined by bound-free scattering. This provides a sensitive dial to fitting the full spectra – both the free-free and bound-free components, as well as the relative strength of the elastic feature, must be matched in order to infer the ionization state.

The absolute intensity of the total electron dynamic structure factor is determined from the integral of the

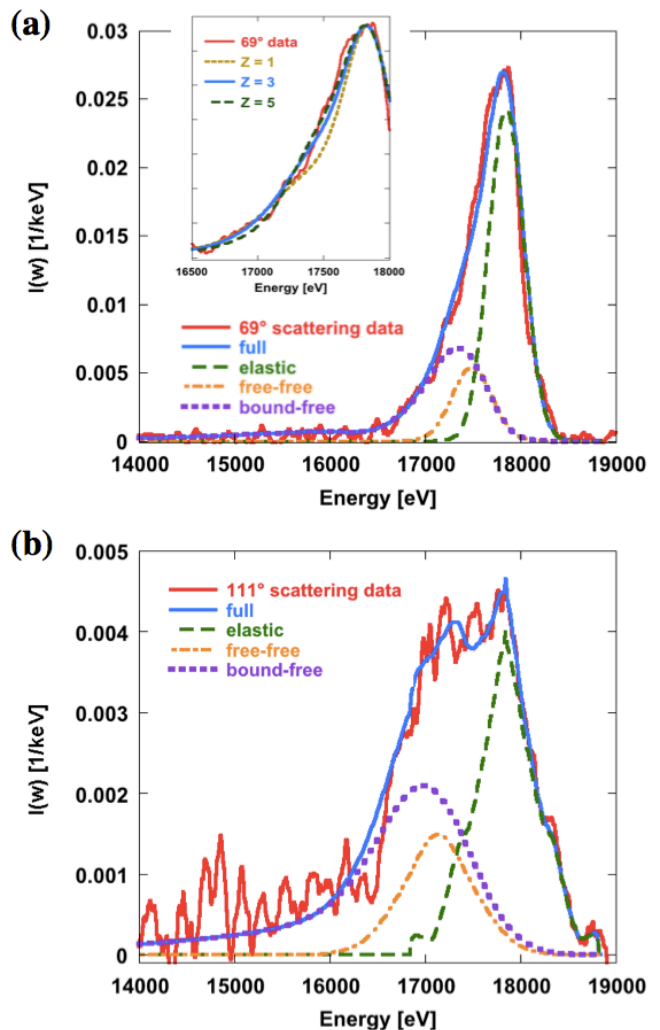


FIG. 2. Examples of x-ray scattering spectra from singly shocked Al for two different scattering angles. The spectrum at 69° is sensitive to the ionization state and provides $Z = 3$ (inset (a)). Best fit for the $\theta = 69^\circ$ (a) and 111° (b) experimental data together with the individual contribution from elastic scattering corresponding to the first term in Eq. (3), inelastic scattering from free electrons (free-free scattering) corresponding to the second term in Eq. (3), and inelastic scattering from bound electrons (bound-free scattering) corresponding to the third term in Eq. (3). The full synthetic x-ray scattering spectrum takes into account the sum of these contributions. The experimental spectra have been background corrected and are plotted in absolute units of intensity of the dynamic structure factor.

spectrally resolved XRTS spectrum for each scattering angle. Corrections are made to the measured scattered power for the polarization of the incident radiation and the length and solid angle of the scattering volume. To obtain absolute calibration, the first frequency moment (f-sum rule) [25] is applied to the 111° data (a high k case where the Compton shift is considerable enough to separate the elastic from the inelastic peak) to derive a

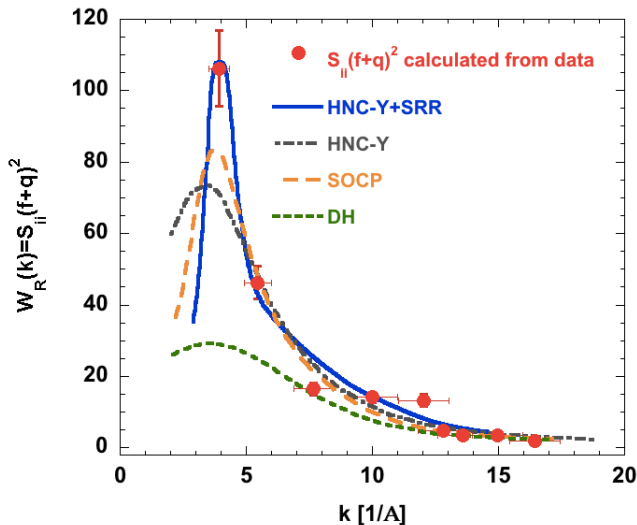


FIG. 3. Elastic scattering amplitude data measured as a function of scattering vector k from shock-compressed aluminum for a density of $n_e = 8.1 \times 10^{23} \text{ cm}^{-3}$ and temperature $T_e = 10 \text{ eV}$. Also shown are various calculations using HNC with quantum potential models of [10] and the analytical SOCP and DH models of [26].

calibration constant. The amplitude of the elastic scattering is then determined by subtracting out the free-free and bound-free components. The free-free contribution is directly calculated from a $S_{ee} = \langle Z \rangle \times 1/(1 + \alpha^2)$ scaling, and the contribution from bound-free transitions is analytically derived as described in Ref. [16].

Figure 3 shows the measured strength of the elastic scattering signal, $W_R(k) = [f(k) + q(k)]^2 S_{ii}(k)$, as a function of scattering vector k for the shock-compressed aluminum with $\rho = 8.1 \text{ g/cm}^3$ and $T_e = T_i = 10 \text{ eV}$ at nine different wave numbers (or scattering angles). A sharp maximum of $W_R(k) = 106$ is exhibited at $k = 4.0 \text{ \AA}^{-1}$, demonstrating the strong ion-ion correlations in the shocked aluminum. Previous measurements of the elastic scattering intensity in low Z materials (e.g., in LiH at much lower pressures of 3–4 Mbar [27]) showed absolute elastic scattering amplitudes of 1.4 and below; here, the experimentally measured peak value is much stronger, with distinct sensitivity to the different theoretical models.

We model the weight of the Rayleigh peak using four different approaches: the Debye-Hueckel (DH) model [26], the screened one component plasma (SOCP) model [26], and via the Ornstein-Zernicke equation using the HNC closure together with a potential incorporating linear screening (Yukawa, HNC-Y) and HNC-Y additionally including short range repulsion (HNC-Y+SRR) [10]. All models incorporate a $\pm 10^\circ$ k -vector blurring for each angle considered, consistent with the geometry of the experiment. Analytical calculations in the form of the DH model, derived for weakly coupled plasmas naturally fail

to capture the clear trend seen in the experimental data, as the DH model cannot describe the strong ion-ion correlations. The SOCP model, which assumes ions are embedded in a polarizable electron gas and, thus, interact via a screened Coulomb potential, predicts a pronounced peak at the right location, with an approximate width of the peak of the correct span, but underestimates the absolute amplitude of the correlation peak. HNC-Y appears to describe screening fairly accurately at large k , but discrepancies arise at the smaller k , where the ion-ion repulsion is underestimated. Only an explicit calculation for strong coupling, the HNC-Y+SRR model for the ion-ion interaction, gives overall good agreement with the experimentally measured data. The HNC-Y+SRR calculation can correctly account for the strong correlations in the system. The excellent agreement with the experimental data demonstrates the importance of the short range repulsion stemming from bound electrons in addition to Yukawa-type linear screening caused by the free electrons.

These calculations also show that the elastic x-ray scattering amplitude peak shifts to higher wave number with increasing density, while the width and peak amplitude provide information on the temperature and ionization state. By doubling the density of the Al (as can be done in a counter propagating shock collision), the ion-ion correlation peak is expected to shift by $\Delta k = 1 \times 10^{10} \text{ \AA}^{-1}$, corresponding to $\Delta \theta = 10^\circ$ in the geometry used in this experiment. As temperature and ionization are varied, the position of the maximum does not vary significantly, but the width of the peak changes. This presents a new diagnostic opportunity to characterize compressed states of matter by wave number resolving the elastic amplitude to complement the findings from the frequency resolved inelastic scattering.

In summary, we have used angularly resolved x-ray Thomson scattering at 17.9 keV to probe a compressed mid- Z material. The experimental data are compared with screening models showing a strong peak characteristic of the warm dense matter state with significantly higher correlations than expected for a compressed plasma state. Screening effects must be accounted for in order to fit the shape and absolute intensity of the data. This demonstrates the capability of XRTS to resolve the ion-ion correlation for an accurate measurement of compression.

This work was performed under the auspices of the U.S. Department of Energy by Lawrence Livermore National Laboratory under Contract DE-AC52-07NA27344. Work was also supported by the Laboratory Directed Research and Development Grant 11-ERD-050 and the National Laboratory User Facility.

-
- [1] M. J. Edwards, J. D. Lindl, B. K. Spears, S. V. Weber, L. J. Atherton, D. L. Bleuel, D. K. Bradley, D. A. Callahan, C. J. Cerjan, D. Clark, et al., *Physics Of Plasmas* **18**, 051003 (2011).
- [2] S. H. Glenzer, D. A. Callahan, A. J. Mackinnon, J. L. Kline, G. Grim, E. T. Alger, R. L. Berger, L. A. Bernstein, R. Betti, D. L. Bleuel, et al., *Physics Of Plasmas* **19**, 056318 (2012).
- [3] D. Riley, N. Woolsey, D. McSherry, I. Weaver, A. Djaoui, and E. Nardi, *Physical Review Letters* **84**, 1704 (2000).
- [4] A. Ravasio, G. Gregori, A. Benuzzi-Mounaix, J. Daligault, A. Delserieys, A. Faenov, B. Loupiau, N. Ozaki, M. R. Le Gloahec, T. Pikuz, et al., *Physical Review Letters* **99**, 135006 (2007).
- [5] E. García Saiz, G. G. Gregori, F. Y. F. Khattak, J. J. Kohanoff, S. S. Sahoo, G. S. G. Naz, S. S. Bandyopadhyay, M. M. Notley, R. L. R. Weber, and D. D. Riley, *Physical Review Letters* **101**, 075003 (2008).
- [6] B. Nagler, U. Zastra, R. Fäustlin, S. Vinko, T. Whitcher, A. Nelson, R. Sobierajski, J. Krzywinski, J. Chalupsky, E. Abreu, et al., *Nature Physics* **5**, 693 (2009).
- [7] H. Sawada, S. P. Regan, P. B. Radha, R. Epstein, D. Li, V. N. Goncharov, S. X. Hu, D. D. Meyerhofer, J. A. Delettrez, P. A. Jaanimagi, et al., *Physics Of Plasmas* **16**, 052702 (2009).
- [8] O. Ciricosta, S. Vinko, H. K. Chung, B. I. Cho, C. Brown, T. Burian, J. Chalupsky, K. Engelhorn, R. Falcone, C. Graves, et al., *Physical Review Letters* **109**, 065002 (2012).
- [9] K. Wünsch, P. Hilse, M. Schlanges, and D. O. Gericke, *Physical Review E* **77**, 056404 (2008).
- [10] K. Wünsch, J. Vorberger, and D. O. Gericke, *Physical Review E* **79**, 010201 (2009).
- [11] S. Glenzer, G. Gregori, R. Lee, F. Rogers, S. Pollaine, and O. Landen, *Physical Review Letters* **90**, 175002 (2003).
- [12] H. J. Lee, P. Neumayer, J. Castor, T. Döppner, R. W. Falcone, C. Fortmann, B. A. Hammel, A. L. Kritcher, O. L. Landen, R. W. Lee, et al., *Physical Review Letters* **102**, 115001 (2009).
- [13] C. Fortmann, H. Lee, T. Döppner, R. Falcone, A. Kritcher, O. Landen, and S. Glenzer, *Physical Review Letters* **108**, 175006 (2012).
- [14] D. Kremp, M. Schlanges, and W.-D. Kraeft, *Quantum Statistics of Nonideal Plasmas* (Springer, 2005).
- [15] J. Chihara, *Journal of Physics: Condensed Matter* **12**, 231 (2000).
- [16] G. Gregori, S. Glenzer, W. Rozmus, R. Lee, and O. Landen, *Physical Review E* **67**, 026412 (2003).
- [17] B. Mattern, G. Seidler, J. Kas, J. Pacold, and J. Rehr, *Physical Review B* **85** (2012).
- [18] T. R. Boehly, R. S. Craxton, T. H. Hinterman, J. H. Kelly, T. J. Kessler, S. A. Kumpan, S. A. Letzring, R. L. Mccrory, S. F. B. Morse, W. Seka, et al., *Review of Scientific Instruments* **66**, 508 (1995).
- [19] M. M. Marinak, G. D. Kerbel, N. A. Gentile, O. Jones, D. Munro, S. Pollaine, T. R. Dittrich, and S. W. Haan, *Physics Of Plasmas* **8**, 2275 (2001).
- [20] K. Fournier, J. Satcher, M. May, J. Poco, C. Sorce, J. Colvin, S. B. Hansen, S. MacLaren, S. Moon, and J. Davis, *Physics Of Plasmas* **16**, 052703 (2009).
- [21] F. Girard, J. P. Jadaud, M. Naudy, B. Villette, D. Babonneau, M. Primout, M. C. Miller, R. L. Kauffman, L. J. Suter, J. Grun, et al., *Physics Of Plasmas* **12**, 092705 (2005).
- [22] A. Pak, G. Gregori, J. Knight, K. Campbell, D. F. Price, B. Hammel, O. L. Landen, and S. H. Glenzer, *Review of Scientific Instruments* **75**, 3747 (2004).
- [23] J. Seely, G. Holland, L. Hudson, C. Szabo, A. Henins, H. S. Park, P. K. Patel, R. Tommasini, and J. Martinlaming, *High Energy Density Physics* **3**, 263 (2007).
- [24] C. Szabo, U. Feldman, S. Seltzer, L. Hudson, M. O'Brien, H. Park, and J. Seely, *Optics Letters* **36**, 1335 (2011).
- [25] S. Ichimaru, *Reviews of Modern Physics* **54**, 1017 (1982).
- [26] G. Gregori, A. Ravasio, A. Höll, S. Glenzer, and S. Rose, *High Energy Density Physics* **3**, 99 (2007).
- [27] A. L. Kritcher, P. Neumayer, C. R. D. Brown, P. Davis, T. Döppner, R. W. Falcone, D. O. Gericke, G. Gregori, B. Holst, O. L. Landen, et al., *Physical Review Letters* **103**, 245004 (2009).